frontiers | Frontiers in Earth Science

ORIGINAL RESEARCH
published: 11 May 2022
doi: 10.3389/feart.2022.880366

Fracture Characterization of Lower Cambrian Niutitang Shale in Cen'gong Block, Southern China

Xinghua Wang[1,2,3], Ruyue Wang[1], Rongtao Guo[1], Arash Dahi Taleghani[3], Shuaitao Su[4], Wenlong Ding[2], Yue Gong[1], Fuqiang Lai[5], Zhonghu Wu[6], Yushan Su[1] and Zhe Cao[1]*

[1]Sinopec Petroleum Exploration and Production Research Institute, Beijing, China, [2]School of Energy Resources, China University of Geosciences (Beijing), Beijing, China, [3]John and Willie Leone Family Department of Energy and Mineral Engineering, The Pennsylvania State University, University Park, PA, United States, [4]Beijing Jiaoen Energy Exploration Co., Ltd., Beijing, China, [5]Chongqing University of Science and Technology, Chongqing, China, [6]College of Civil Engineering, Guizhou University, Guiyang, China

The marine shale of southern China is characterized by old sedimentary formations, multiple tectonic activities, and poor preservation conditions. The fracture system in this shale reservoir is extraordinarily complex, greatly adding to difficulties for shale gas exploration and development. Based on field surveys, drilling cores, seismic data interpretation, and experimental tests, we try to characterize the developmental characteristics of shale fractures at different scales and delineate the stages of fractures in the Cen'gong block. The results show that the Cen'gong block is a saddle-shaped structure formed by the northeast-oriented Banxi anticline and the southwest-oriented Lannigan anticline. There are four types of core fractures developed in the study area, namely, pyrite-filled fractures, fibrous veins, subvertical fractures, and slip fractures, and the forming time of these fractures are later in turn based on the intersecting relationships and analysis of filling minerals. The fracture rose diagram and the paleomagnetic orientation experiments indicate that the fracture direction is mainly NNE and partly NW, consistent with the direction of faults identified in the seismic data. Quantitative statistics have been conducted for fracture aperture, length, and density distribution. The fracture abundance has a close relationship with buried depth and regional faults in the study area.

Keywords: shale, fracture characterization, lower Cambrian, natural fractures, Cen'gong block

OPEN ACCESS

Edited by:
Lei Gong,
Northeast Petroleum University, China

Reviewed by:
Yahao Huang,
Yangtze University, China
Chen Zhang,
Chengdu University of Technology, China

****Correspondence:***
Ruyue Wang
wry1990@vip.qq.com

Specialty section:
This article was submitted to Structural Geology and Tectonics, a section of the journal Frontiers in Earth Science

Received: *21 February 2022*
Accepted: *04 April 2022*
Published: *11 May 2022*

Citation:
Wang X, Wang R, Guo R, Dahi Taleghani A, Su S, Ding W, Gong Y, Lai F, Wu Z, Su Y and Cao Z (2022) Fracture Characterization of Lower Cambrian Niutitang Shale in Cen'gong Block, Southern China. Front. Earth Sci. 10:880366. doi: 10.3389/feart.2022.880366

1 INTRODUCTION

According to the reports from China's Ministry of Natural Resources and the U.S. Energy Information Administration, China has the richest known reserves of shale gas in the world. However, now in China, the commercial production of shale gas has only been carried out in Changning, Weiyuan, Zhaotong, Jiaoshiba, and other areas in the Sichuan Basin aiming at the Lower Silurian Longmaxi shale (Dong et al., 2018; Wang R. et al., 2019). Various degrees of exploration have been carried out in other shale formations but have not led to considerable production or a development plan yet. It is partly due to the fact that the marine shale in southern China has its own complexities, which is mainly driven by old sedimentary formations, high thermal evolution, many periods of tectonic movements, complex tectonic deformations, complex stress state, and large differences in hydrocarbon accumulation systems (Jin and Cai, 2006; Kang, 2012; Jia et al., 2016; Wang R. Y. et al., 2020, 2022; Zhou et al., 2022).

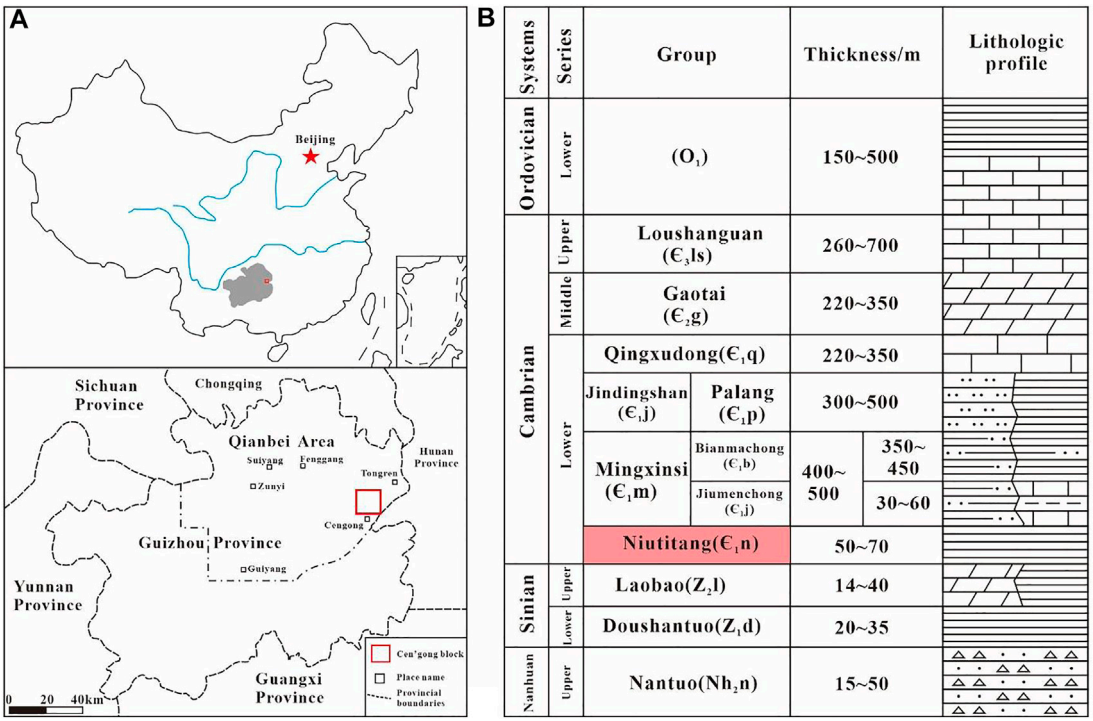

FIGURE 1 | (A) Location of Cen'gong block; **(B)** stratigraphic column of the study area.

Additionally, matrix pores in shale reservoirs basically cannot be effective seepage channels because of low porosity and permeability. Economic oil and gas production can only be achieved by reservoir stimulation such as hydraulic fracturing using the experience of shale gas exploration and development in other countries around the world (Dong et al., 2014; Dahi Taleghani and Olsen., 2011; Ding et al., 2015; Sheng and Li, 2016; Cai and Dahi Taleghani, 2019; Cao et al., 2021; Liu et al., 2021; Wu et al., 2017, 2022). As a key parameter influencing the effectiveness of hydraulic fracturing, natural fractures and their characteristics are crucial. Natural fractures not only serve as the storage space of gas but also provide an effective seepage channel for gas migration (Wang R. Y. et al., 2018, Wang et al., 2018 X., 2021; Dong et al., 2018; Zhang et al., 2020). Natural fractures can be reactivated during hydraulic fracturing and directly affect the direction, angle, and treatment pressure during hydraulic fracturing. Hydraulic fracturing, if designed properly, may facilitate the connectivity of fracture networks and extends the drainage area due to fracturing (Dahi Taleghani and Olsen., 2011; Guo et al., 2014; Chen et al., 2021; Lan et al., 2021). On the other hand, too many large natural fractures may destroy cap rocks and connect to caverns, faults, and underground water networks, causing the gas to escape. It may also lead to well leakage, well collapse, and water flood during hydraulic fracturing.

At present, there are few studies on the forming time and activity history of shale fractures in southern China. Fractures' characteristics are not studied comprehensively, and there is a lack of relevant studies on fracture patterns. Therefore, based on seismic data interpretations, field observations, and core descriptions, we try to characterize fractures of the marine shale in Cen'gong block, Guizhou Province, China. This study provides basic data for the next step of field development such as well layout optimization, drilling plans, and design of hydraulic fracturing jobs in the Cen'gong block.

2 GEOLOGICAL SETTING

The Cen'gong block is located in the eastern part of Guizhou Province, China, covering an area of about 914 km^2 (**Figure 1A**). The target gas-bearing shale formations are Niuhuitang shale and Bianmachong shale of Lower Cambrian. So far, the interpretation work of about 487 km of 2D seismic data and 26.2 km^2 of 3D seismic data has been completed, and four drilling wells, namely, CY-1 well, TX-1 well, TM-1 well, and CD-1 well have been drilled. Among them, TX-1 has been drilled to a depth of 1897.67 m, the thickness of Niutitang shale is more than 60 m, and the gas content is 2.16 m^3/t on average. It is cautiously predicted that the original gas in place (OGIP) in Niuhuitang shale is about 147.7 billion cubic meters, and the OGIP in Bianmachong shale is 40–60 billion cubic meters. The sedimentary strata in the Cen'gong block mainly include Nantuo formation (Nh_2n) of the upper Nanhua system, Doushantuo formation (Z_1d) and Laobao formation (Z_2l) of Sinina, and Niuhuitang formation ($Є_1n$), Jiumenchong formation ($Є_1j$), Bianmachong formation ($Є_1b$), Palang formation ($Є_1p$), Qingxudong formation ($Є_1q$), and Gaotai formation ($Є_1g$) of Cambrian. Thereinto, the $Є_1b$ can be divided into $Є_1b^1$ (the lower member of the Bianmachong

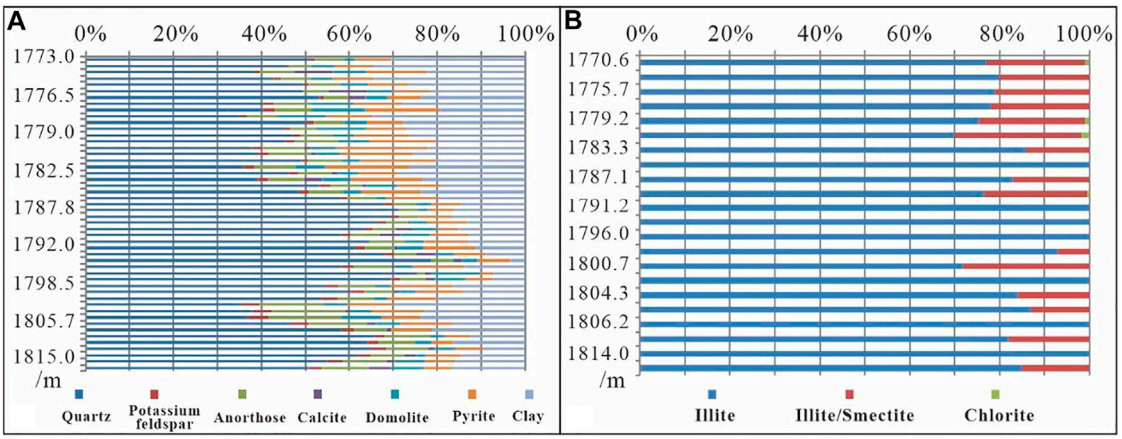

FIGURE 2 | Mineral composition and content of Niutitang shale **(A)** and clay minerals **(B)** in TX-1 well.

formation), $\epsilon_1 b^2$ (the middle member of the Bianmachong formation), and $\epsilon_1 b^3$ (the upper member of the Bianmachong formation) (**Figure 1B**).

The lithology of the Niutitang formation is mainly gray–black siliceous shale, referred to as Niutitang shale. Specifically, the bottom of Niutitang shale is a black siliceous rock, interbedded with phosphorite and black high-carbonaceous shale. The lower part is interbedded with gray–black calcareous shale, gray mud siltstone, and gray–black mudstone, and few star-shaped pyrites are developed. The upper part is a gray mudstone, and there are some calcite layers occasionally. The organic matter in Niutitang shale is mainly sapropelic and amorphous, and the source of which is mainly algae and other low brackish water aquatic organisms. The kerogen types of organic matter are type I and II in major, which have a good hydrocarbon production capacity. With deepening depth, the TOC (Total Organic Carbon) content increases first and then decreases gradually. The bitumen reflectivity is between 2.5 and 3.8%, within the mature and overmature stages. The illite crystallinity is between 0.33° and 0.52°, indicating that Niutitang shale is in the very low metamorphic zone and the late metamorphic stage.

RD (X-ray diffractometer) analysis of core samples in Niutitang shale shows that the content of brittle minerals ranges from 28.7 to 95.5%, with an average content of 62.06%. The brittle minerals are mainly quartz with an average content of 44.3%, followed by feldspar with an average content of 8.4%, dolomite and calcite with an average content of 4.6 and 1.2%, respectively, and pyrite with an average content of 6.3%. The content of clay minerals ranges from 4.5 to 71.4%, with an average content of 34.6% (**Figure 2**). The clay minerals are mainly illite, containing a small amount of chlorite and illite–smectite mixed layer. In summary, the brittleness of Niutitang shale is very good.

3 METHODS

There are four drilling wells analyzed for this study, i.e., TX-1, TM-1, CY-1, and CD-1, all drilled in the Cen'gong block. Niutitang shales in these four wells are all encountered and completely cored with the same information on thickness and lithology. In order to study the fracture abundance and characteristics, every fracture was accurately measured by rulers. Core photographs of every fracture were also examined for characterization of the fracture types and crosscutting relationships. To distinguish the calcite and quartz filled in fracture, 15% HCl and scratch tests were used. The pyrite was mainly identified by the color.

Some core samples with filled fractures were selected and ground into thin sections, which were observed using OM (optical microscope) and SEM (scanning electron microscope) for characterizing the microfractures. Others were made into a cylindrical shape for the paleomagnetic orientation tests. The SEM used is a field-emission gun, 200F model of FEI company, which provided a greater depth of field and a clearer picture of micropores and fractures. The inspection was conducted at 35% RH and 24°C.

The geologic sections of multiple outcrops were measured for analyzing sedimentary stratigraphy and outcrop fracture characterization. We photographed and collected information of the outcrop fractures and mapped rose diagram to analyze fracture orientation. We also conducted paleomagnetic orientation experiments to comprehensively determine the direction of fracture extension.

The paleomagnetic orientation method, an important method for analyzing fracture orientation, not only takes a direct measurement on drilling cores but also has a high accuracy of orientation. The theory is that the direction of the viscous remanence of the core can be determined by thermal demagnetization or alternating demagnetization, which is consistent with the direction of the modern geomagnetic field. Then, the relative direction of the fracture in the core can be obtained after calculation and correction.

The first step of this experiment was the collection and processing of paleomagnetic experimental samples. We marked the primary marker lines parallel to the target fracture on the core, and then drilled cylindrical samples (**Figure 3**). A

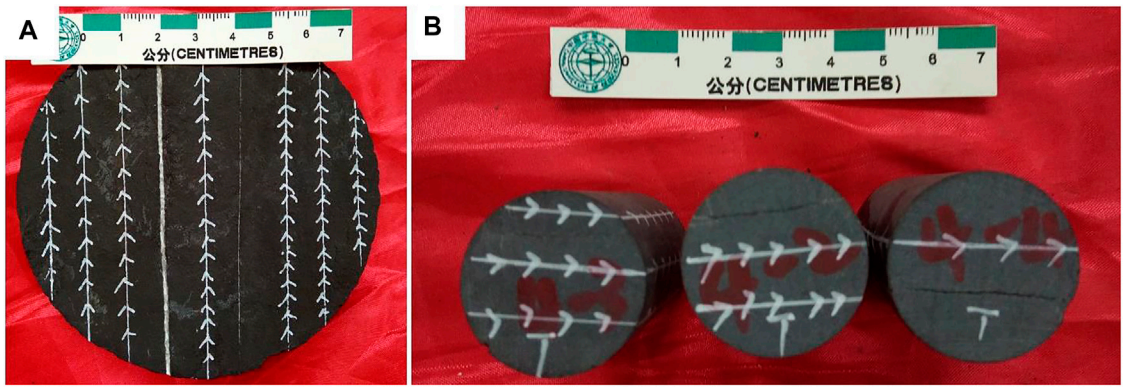

FIGURE 3 | Core samples for paleomagnetic orientation experiments; marker lines are parallel to the target fracture. **(A)** Original core sample; **(B)** Cylindrical samples after processing.

coordinate system for the experimental sample was constructed by marking a secondary marker line on the cylinder surface in the direction of the primary marker line. The second step was paleomagnetic testing. Because organic matter was rich in shale, alternating demagnetization was selected for avoiding changing the magnetic state of the samples due to high-temperature heating during thermal demagnetization. Each sample was processed at the Laboratory of Paleomagnetism in the China University of Geosciences (Beijing) using the ASC IM-10-30 pulsed magnetometer. The applied alternating demagnetization strengths were 2.5, 5, 7.5, 10, 12.5, 15, 20, 25, 30, 40, 50, 60, 70, 80, 90, and 100 mT in order. After each alternating demagnetization, we measured the remanence of the sample and recorded the experimental results using the AGICO JR-6A rotational magnetometer. The final step was processing and interpreting the experimental data. The average magnetic declination and magnetic inclination of viscous remanence were calculated by professional software, which was oriented with respect to the sample coordinate system. By correcting this, we can finally obtain the direction of the main marker line (the natural fracture) in the present geographic system.

4 RESULTS

4.1 Regional Structure Characteristics

According to the seismic interpretation, the Cen'gong block is a saddle-shaped structure formed by the northeast-oriented Banxi anticline and the southwest-oriented Lannigan anticline (**Figure 4**). The Changchong syncline to the east and the Guanzhai syncline to the west further highlight the saddle-shaped features. Second, faults are associated with the distribution of anticline and syncline, which are mainly located in the hinge zone of most folds such as Guanzhai syncline, Banxi anticline, Changchong syncline, and Lannigan anticline. Additionally, most of the faults are along the NE and NNE direction, a few of which are in the EW direction. This is consistent with the regional geotectonic setting. The large faults mainly include the Daozhanping fault, Shuwei fault, Tongluo fault, Nangfangping fault, Shuiyinchang fault, and Minhe fault, which directly control the saddle-shaped structural framework of the Cen'gong block and also affect the distribution and characteristics of the secondary faults.

Additionally, the Shuiyinchang fault and the Nongchangping fault break the Guanzhai syncline along the northeast–southwest direction iteratively, and the Tongluo fault, the Shuiwei fault, and the Daochenping fault also break the Changchong syncline along the northeast–southwest direction iteratively. The Changchong syncline and Guanzhai syncline are characterized by obvious belted structures because of these faults. At the center of the Cen'gong block, the stratigraphy is gently undulating, and small faults are more developed rather than large faults. In addition, the faults show a characteristic of increasing development when they approach anticlines in the north and south.

From the EW496 and SN500 seismic lines, the thickness of the Niutitang shale is in good continuity within the Cen'gong block (**Figure 5**), mainly between 50 and 70m, However, all the strata are affected by fractures and folds, and their burial depths vary, specifically increasing firstly and then decreasing from south to north. The overall pattern is shallow buried in the north and south, deep buried in the east and west, and moderately buried in the block center. It can be seen that the stratum is greatly affected by north and south folds, where Niutitang shale is exposed to the ground, while the stratum is greatly affected by east and west faults, where Niutitang shale is deeply buried.

4.2 Fractures in Outcrops

The lower Cambrian sedimentary strata, including the Niutitang shale exposed in the northern, southern, and eastern parts of the study area, and three geologic sections were measured in Xiaobao, Banxi, and Huangdao outcrops, and the outcrop fractures of Niutitang shale were finely characterized. It is widely developed for small folds and faults in these outcrops, which shows that the area suffered complex tectonics. Fracture characteristics in these three geologic sections are similar; here, we just take Xiaobao geological section as an example to analyze fractures in outcrops.

In Xiaobao geological section, the black carbonaceous shale and siliceous shale are frequently interbedded, and siliceous nodules are well developed (**Figure 6**). The morphology and

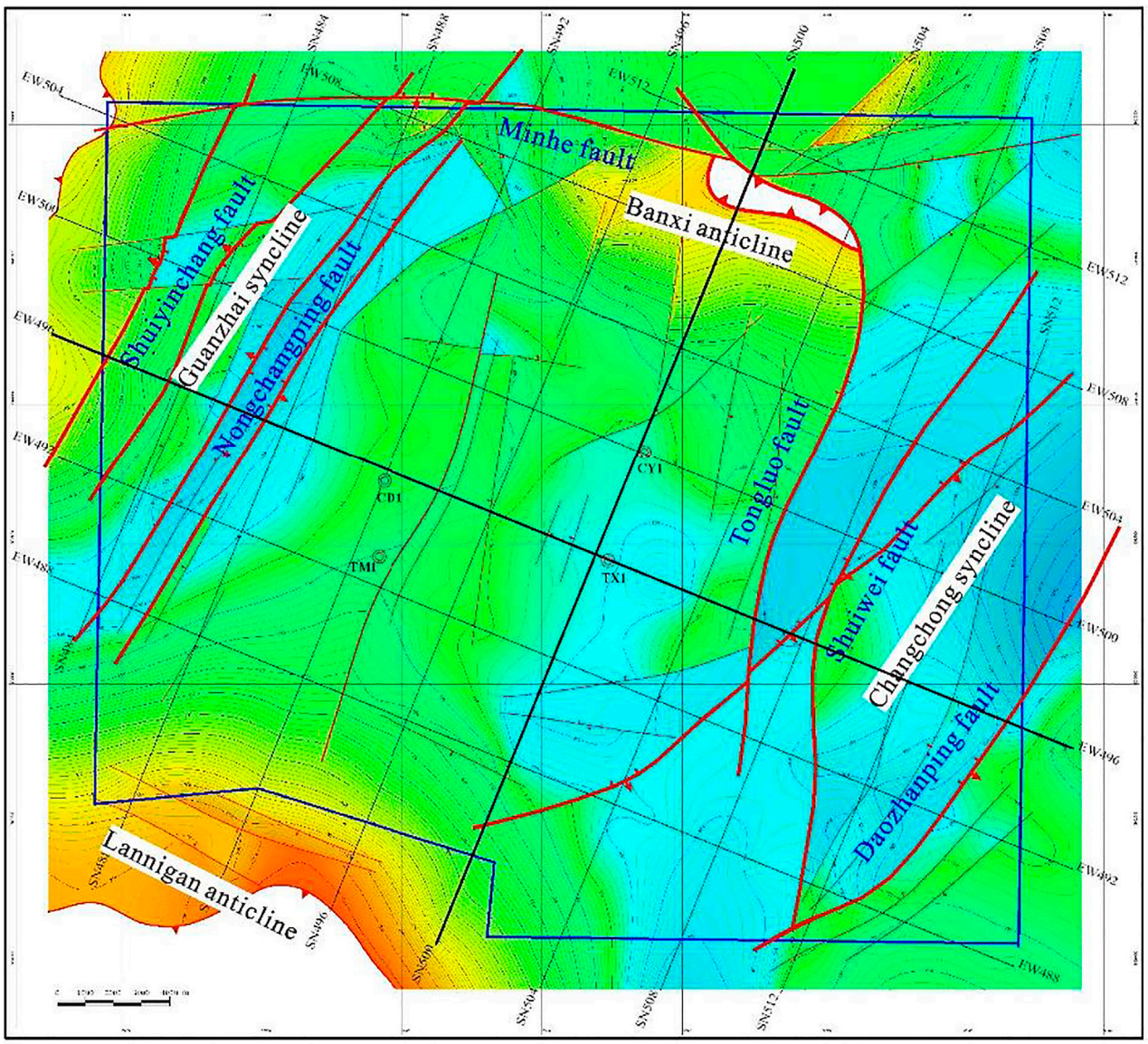

FIGURE 4 | Geological structure and faults map of Niutitang shale in Cen'gong block.

size of these nodules are diverse, the shapes are mostly ellipsoidal and spherical, and the long axis directions are parallel to the stratigraphic distribution direction. The fractures in Xiaobao geological section are mainly fold-fault-related fractures, bedding fractures, slip fractures, and regional fractures. The fold-fault-related fractures refer to fractures related to small local structures such as folds or faults, and they can be subdivided into fault-related fractures or fold-related fractures. These fractures are mainly opening-mode fractures with large aperture and high dip angle, and their extension directions are mostly limited by the local faults and folds. Additionally, the shale usually has high clay minerals content and well-developed beddings, and its weathering resistance is weak. When it is subjected to long-term exposure to the sunshine, wind, and other weathering effects as well as mechanical compaction, water-loss contraction, and other geological effects, it is prone to form bedding fractures along the original lamination surface or small-scale lithological interfaces after physical and chemical breakage (Wang et al., 2016). There is no doubt that frequent interbedding of black carbonaceous shale and siliceous shale in the Xiaobao geological section further promotes the formation of the bedding fractures. But the abundance of bedding fractures varies in different areas because of the inhomogeneous weathering effect.

Slip fractures are a series of fractures formed by shear stress parallel to the bedding plane of shale under the extensional or compressive tectonic effect. They are often characterized by obvious slickensides and steps, indicating obvious slippage between layers. Slip fractures are common in plastic thick-bedded shales. Their extension directions are mostly parallel to

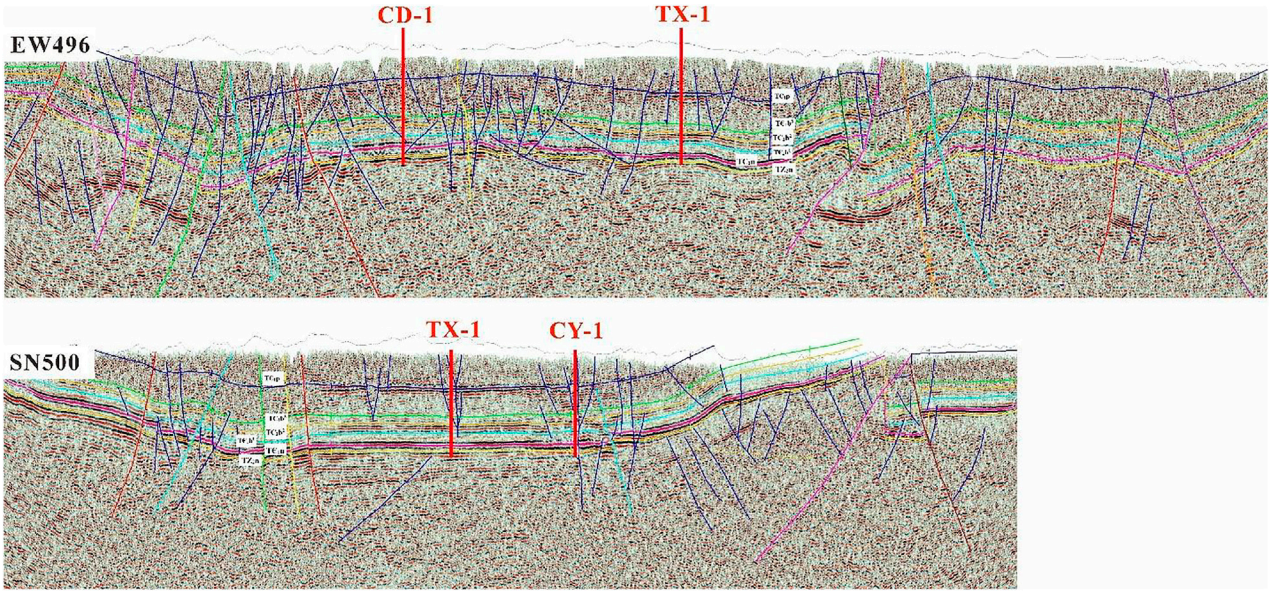

FIGURE 5 | 2D seismic interpretation sections across wells in Cen'gong block, and the location was marked in **Figure 4**.

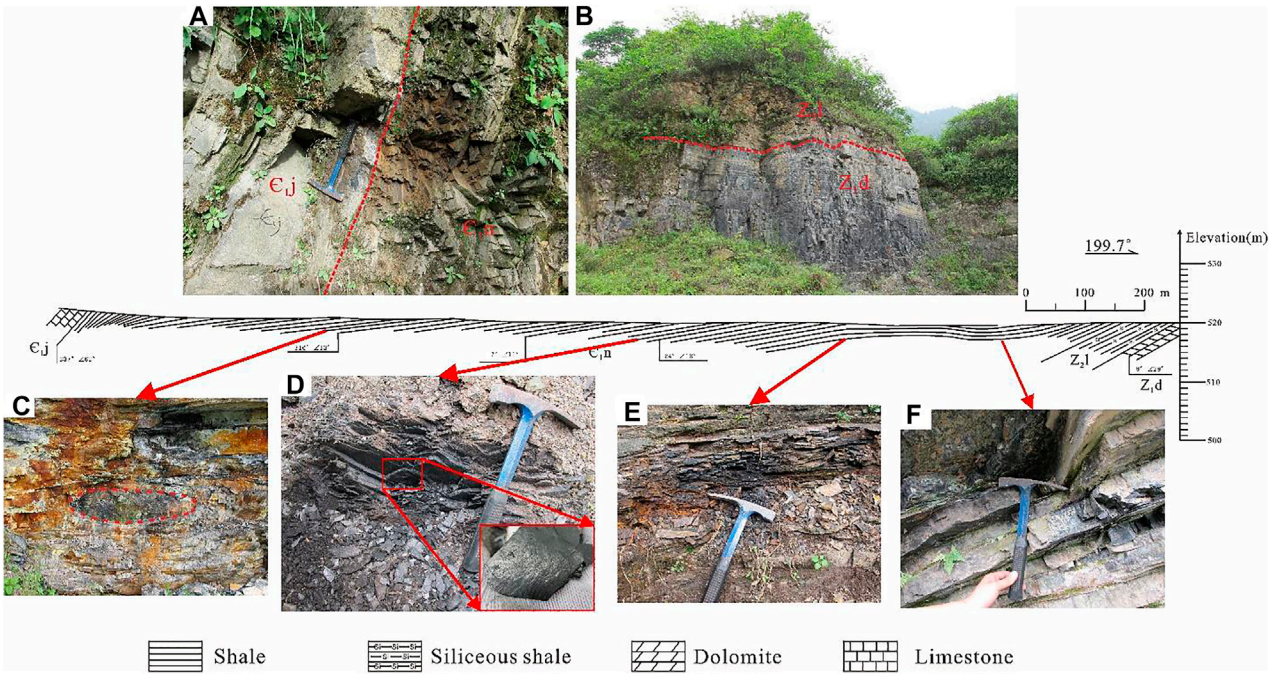

FIGURE 6 | Xiaobao geological section in Cen'gong block.

the shale bedding plane, so the dip angles are usually small. They are mainly distributed at the top and bottom of the shale strata where they are close to other lithologic strata (**Figure 6D**). Regional fractures are generally straight and widely spaced with a long extended distance. They can cut through different sedimentary at a vertical or large angle (Wang et al., 2016; Wang et al., 2018 R. Y.; Wang et al., 2018 X.). Their extension directions can reflect the state of the regional geostress field at the forming time. Besides, regional fractures can control the flow of subsurface fluids, such as water, mineralizing fluids, and geothermal fluids, which are of great practical importance for potential oil and gas reservoirs (English, 2012). Typical regional fracture

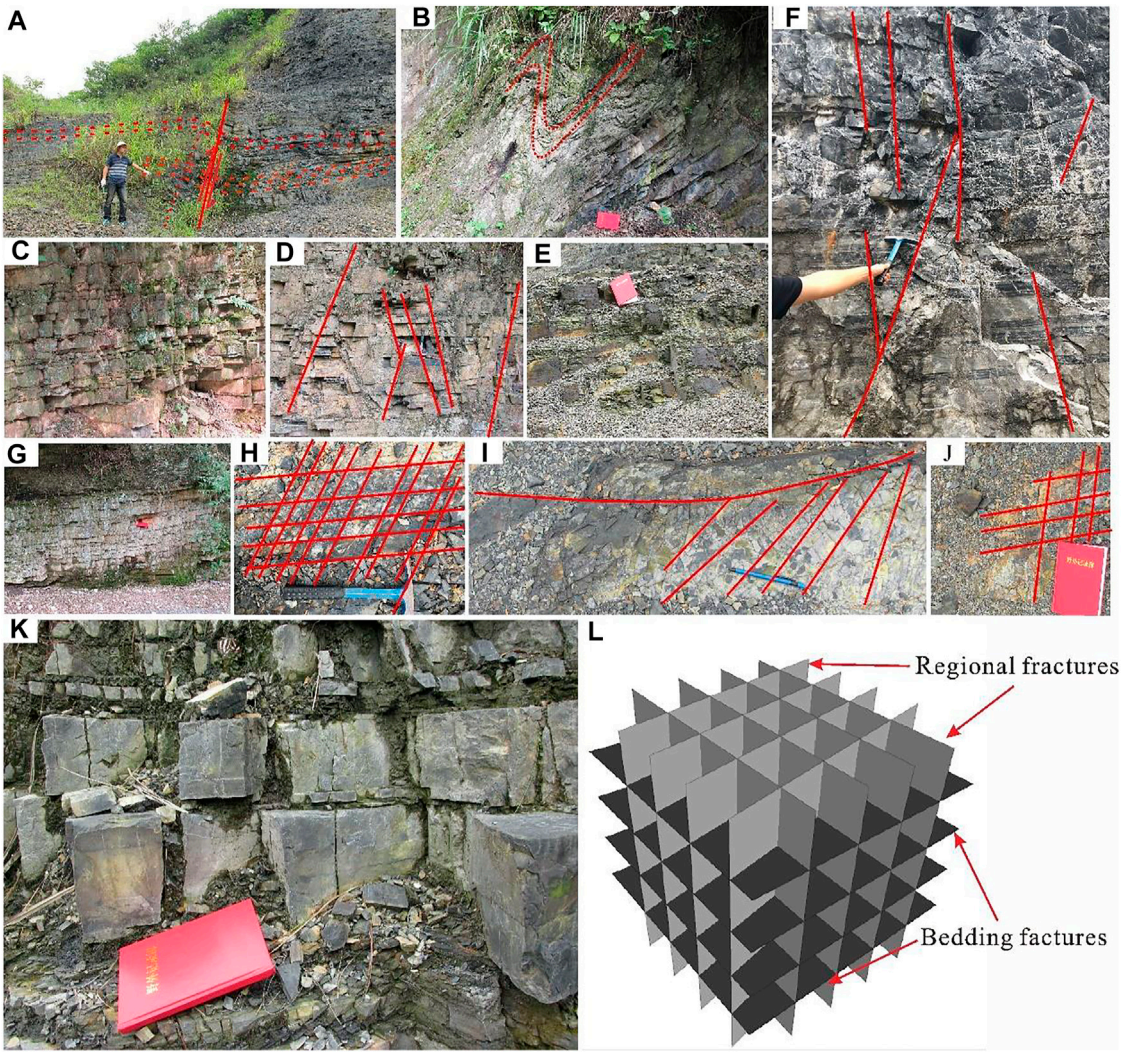

FIGURE 7 | Outcrop fracture characteristics in the Xiaobao geological section of Cen'gong block. **(A)** Fault-bend folds and related fractures; **(B)** slip fold between layers and related fractures; **(C)** bedding fractures; **(D)** high dip angle fractures cutting bedding factures; **(E)** regional fractures; **(F)** high dip angle fractures; **(G)** bedding fractures develop differently in different layers; **(H)** regional fractures in a grid pattern; **(I)** plumose fractures; **(J)** two groups of fractures cutting off each other; **(K)** regional fractures and bedding fractures; **(L)** 3D schematic diagram showing the regional fractures and bedding fractures.

(**Figure 7H–L**) is shown in the Xiaobao section. In total, two sets of regional fractures are observed to cut through each other simultaneously, and they combine with horizontal bedding fractures forming a grid-like pattern on the ground.

4.3 Fractures in Cores

4.3.1 Fracture Types

The Cen'gong block has four drilling wells with Niutitang shale cored including CY-1 well, TX-1 well, TM-1 well, and CD-1 well, each of which has developed a large number of natural fractures. Comparing the four cores in lateral correlation, the paper summarizes four types of natural fractures in Niutitang shale, namely, pyrite-filled fractures, fibrous veins, subvertical fractures, and slip fractures, from the fracture size, occurrence, formation mechanical mechanism, and filled minerals (**Figure 8**).

Pyrite-filled fractures refer to fractures filled by pyrite spreading horizontally along the shale bedding planes or lithologic interfaces, which usually extend beyond the measurement range of cores. The aperture varies, generally ranging from 0.1 to 5 mm. Pyrite-filled fractures are obviously controlled by the lithology, which is usually and widely distributed in gray and black shale layers with rich organic matter. Pyrite is a common mineral component in shale, which generally develops in the shape of a strawberry, needle, or self-shaped crystal (Wang X. et al., 2019). Pyrite accounts for about 3.2–17.2% in shale mineral components of TX-1 well in the Cen'gong block, and the average value can reach 9.8%. The formation of pyrite is closely related to the source and concentration of sulfur in the formation and the pH of the formation water, and the chemical reaction involves three

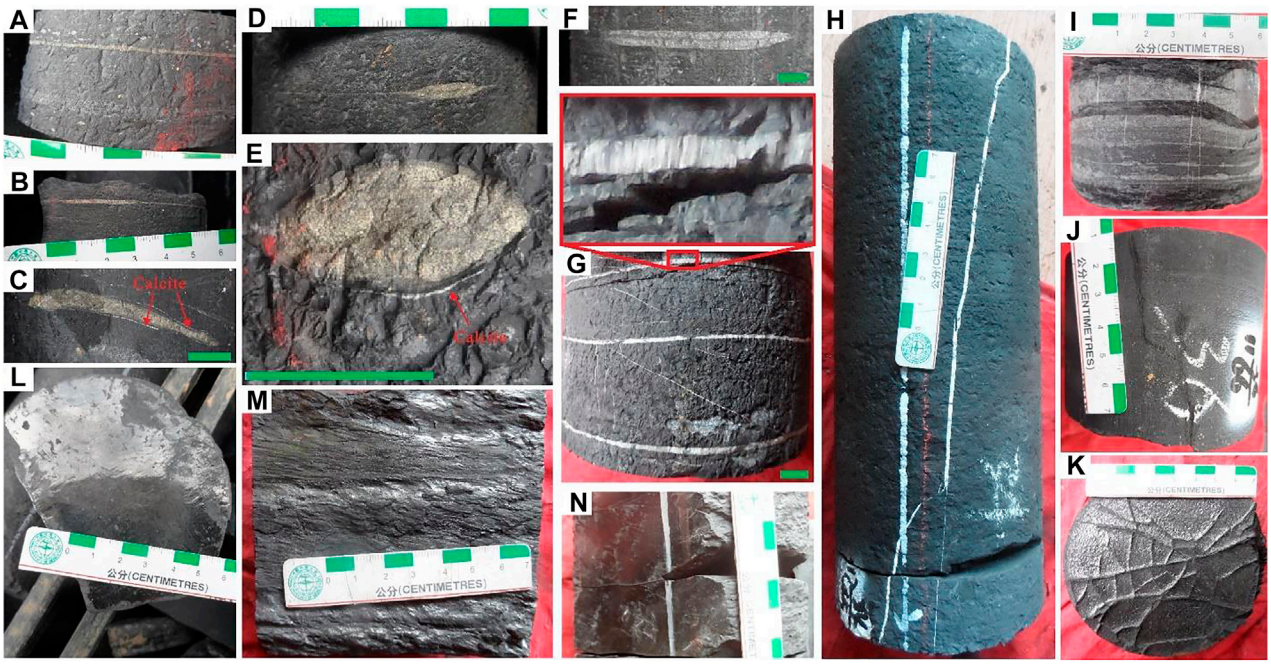

FIGURE 8 | Fracture types and characteristics of Niutitang shale cores in Cen'gong block. **(A)** Straight pyrite-filled fracture; **(B)** horizontal pyrite-filled fracture with changed aperture; **(C)** long strip of pyrite nodule surrounded by calcite-filled fractures; **(D)** lens-shaped nodule with long and short tips; **(E)** spindle-shaped pyrite nodule with calcite-filled fractures at the bottom; **(F)** bedding-parallel fibrous veins with obvious dark trails of host rock; **(G)** bedding-parallel fibrous veins, and the filling mineral calcite is arranged in a comb shape; **(H)** subvertical calcite-filled fractures, and uneven fracture surface means the changes of fracture propagation direction; **(I)** fracture aperture changes a lot when cutting off multilayers; **(J)** vertical clay-filled fracture with changed propagation directions; **(K)** net-shaped fractures with clay and calcite filled fracture; **(L)** horizontal slip fracture with typical mirror structure; **(M)** vertical slip fracture with step structure; **(N)** vertical slip fracture with mirror structure.

main mechanisms: 1) $H_2S + FeS = FeS_2 + H_2$; 2) $FeS + S_5^{2-} = FeS_2 + S_4^{2-}$; 3) sulfation and replacement of iron oxides. In this process, biological activities such as bacteria play a crucial role, significantly accelerating the reaction rate, while organic matter can provide a good culture medium for sulfur-reducing bacteria. Thus, the enrichment of organic matter and secretions from living organisms are thought to be conducive to pyrite formation (Gregory et al., 2019), which is the reason why layered pyrite is widely distributed in organic-rich shale formations.

In addition, pyrite is also often found as nodules in shales. Some of them are in the shapes of spheres, ellipsoids, lenses, etc., and the length ranges from about 1 to 10 cm. It is usually thought of pyrite has an obvious shape change during the diagenetic stage. In the early stage of the sedimentary process, the strata are soft and anisotropic, the pyrite usually grows in spheres. As sedimentation and compaction further intensified, the original spherical pyrite was deformed to some extent, and halo-shaped structures were formed around it. In the late diagenetic stage, pyrite transformed into an ellipsoidal or banded shape along the stratigraphic interface due to increasing impermeability, viscosity, and anisotropy of the strata (Seilacher, 2001). The development of pyrite nodules of various shapes in the study area reflects the changes in the compaction and porosity permeability of the stratum. We can also speculate the location, direction, and magnitude of the force acting on pyrite nodules according to the relationship between the nodule shape and other microstructures. **Figure 8D** shows that the pyrite-filled fractures extend from both tips of the lens-shaped nodule along the shale bedding plane, indicating the direction of growth but limited by the growth and expansion capacity of the pyrite. Only one dominant branch usually develops on both sides of the nodules.

Fibrous veins have a pronounced fibrous structure, and most of them are filled with calcite, so they are also called fibrous calcite veins (**Figures 8F, G**). Like pyrite, calcite is not only an important part of shale mineral composition but also the main fracture filling material. Based on the location of the growth interface and growth direction of the fibrous veins, they can be divided into three types of structures: stretched veins, syntaxial veins, and antitaxial veins (Bons and Montenari, 2005). The aperture of the fibrous veins in the study area ranges from 1 to 5 mm, and the length is usually greater than 10 cm because most fibrous veins extend out of the core along the shale bedding plane. Some short fibrous veins are typically arranged in an en echelon pattern or spread densely parallel to each other. In addition, it is obvious that the fibrous veins are influenced by later compaction, diagenesis, and tectonic activity, which lead to offset, discontinuity, and shortening along the horizontal direction. The fibrous minerals usually have a clear boundary with the surrounding wall rocks, and most of them are normal to the wall rocks in a combed shape. There is also a clear gray–black line in the middle of the vein, and it is the early growth interface that belongs to wall rocks where the crystal of the fibrous veins begins to grow.

Subvertical fractures are the most developed, numerous, and complex fractures in the study area (**Figures 8H–K**). Most of these fractures are filled with calcite, some are filled with dolomite, clay, quartz, or co-filled with multiple minerals. Subvertical fractures without filling minerals are rarely observed (Wang et al., 2017). Dip angles between subvertical fractures and shale bedding plane range from 70° to 90°, the aperture varies greatly, from a few millimeters to several centimeters. Some subvertical fractures are smooth and straight with long extension distance and stable occurrence, which are mainly shear fractures formed under the extrusion or shear tectonic stress. However, most subvertical fractures are often turned, broken, or bifurcated, with short extension distance and big changes in aperture, which are mainly tensile fractures formed under the action of local extension tectonic stress. This kind of fracture is more common at the location where the lithology has a big change. Usually, subvertical fractures have larger apertures in brittle shale intervals such as siltstone, while when they extend to mudstone or shale, the fractures change the directions or terminate abruptly, and the apertures also become smaller. This is related to the petrophysical properties of different lithology intervals. In addition, the subvertical fractures usually cut through each other, which formed an obvious network structure on the sedimentary laminae.

The characteristics of the slip fractures in the core are basically consistent with those observed in the outcrops, which are mainly developed in the thick mudstone and shale with good plasticity, especially in the contact position between the shale and sandstone interlayer. Most of the slip fracture surfaces are undulating and uneven, with large variations in occurrence, and the characteristics of slickensides, scuff marks, and steps are more typical (Fig. 8L–N). Many of the slip fractures are not filled with minerals, and the fracture surfaces are often coated by mineral fibers and carbonaceous debris, which make hands dirty easily.

Previous studies on slip fractures usually classified them as bedding-parallel, low-angle fractures along sedimentary laminae, or lithologic partitioning interfaces (Zeng and Xiao, 1999; Zhang and Yuan, 2002), but this time, by observing a large number of slip fractures in the study area, we found that many subvertical slip fractures were developed in Niutitang formation which cut across the shale laminae. Compared with bedding-parallel slip fractures, subvertical slip fractures have more prominent features such as slickensides and steps. It has shown several directions for scuff marks along the two surfaces of slip fracture. Some are parallel to the laminae, some are oblique to the laminae, and some are perpendicular to the laminae, which indicates the different relative movement of rocks on both sides of the slip surface. From the viewpoint of the genesis mechanism, bedding-parallel slip fractures are mainly formed along mechanical layer boundaries such as shale laminae or thin beds under the action of horizontal shear stress, while subvertical slip fractures are formed along subvertical interfaces such as pre-existing fractures in high dip angle under the action of subvertical shear stress. In addition, compared to the common subvertical shear fractures, subvertical slip fractures have obvious slickensides, which also serve as the most important classification marker in the study to classify these two types of fractures.

4.3.2 Fracture Aperture and Length

Fracture aperture and length are the key factors in determining fracture porosity, permeability, hydrocarbon reserves, and directly evaluating the impact of fractures on development effectiveness. Fractures can usually be viewed as three-dimensional entities with length, width, and height, and the aperture refers to the width between two fracture walls. Since fractures are often filled with cement, their aperture also indicates the width of the cement. Fracture length in this study refers to the extension length or incise depth of a fracture. Due to the limitations of observation angle, location, and range, the length and width of a fracture usually cannot be correctly discerned, and thus it is considered that the side with the longer extension distance represents the length of the fracture. Specifically, for subvertical or vertical fracture, the length refers to incise depth in the longitudinal direction; for bedding-parallel fractures or fractures with low dip angle, the length refers to the extension length in the transverse direction.

The fracture apertures and lengths in the study area change greatly, ranging from a few microns in microscopic fractures to tens of meters in outcrop fractures (**Figure 9**). Because the observation range of microscopic fractures and outcrop fractures is limited, this study uses the observation results of fractures in drilling cores to characterize the fracture parameters. By the observation of 1866 core fractures in TX-1 well, the results show that there are 187 fractures with an aperture less than 0.2mm, 776 fractures with an aperture greater than 0.2 mm and less than 0.5 mm, 528 fractures with an aperture greater than 0.5 mm and less than 1 mm, and the remaining 375 fractures with an aperture greater than 1 mm; there are 1333 fractures with length less than 5 cm, 390 fractures with length greater than 5 cm and less than 10 cm, 138 fractures greater than 10 cm and less than 20cm, and 5 fractures greater than 20 cm. By observing 4883 core fractures in TM-1 well, the results show that there are 663 fractures with an aperture less than 0.2 mm, 1875 fractures with an aperture greater than 0.2 mm and less than 0.5 mm, 1888 fractures with an aperture greater than 0.5 mm and less than 1 mm, and 457 fractures with an aperture greater than 1 mm. There are 1,879 fractures with a length less than 5 cm, 2400 fractures with a length greater than 5 cm and less than 10cm, and 604 fractures with a length greater than 10 cm. The statistics of core fractures in two drilled wells, TX-1, and TM-1, show that the core fracture apertures are mainly less than 1 mm, and lengths are less than 10 cm.

4.3.3 Fracture Density

Fracture density is an important parameter to reveal the fracture abundance, it is often expressed in three main ways: line density, area density, and volume density. Fracture line density refers to the number of fractures in a unit length, fracture area density refers to the cumulative length of fractures in a unit area, and fracture volume density refers to the ratio of the total surface area of observed fractures to a unit volume. The comprehensive histogram of fracture density of a single well can well show the characteristics of the variation of fracture development with drilling depth, which is conducive to comparative analysis with

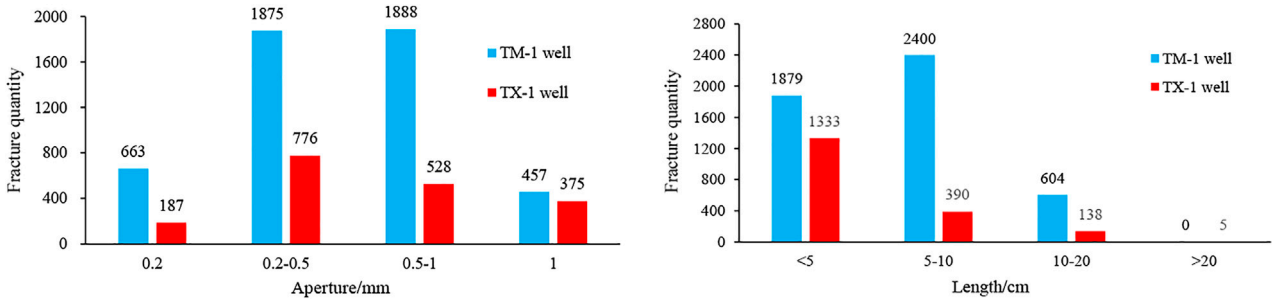

FIGURE 9 | Fracture aperture and length histogram of Niutitang shale in Cen'gong block.

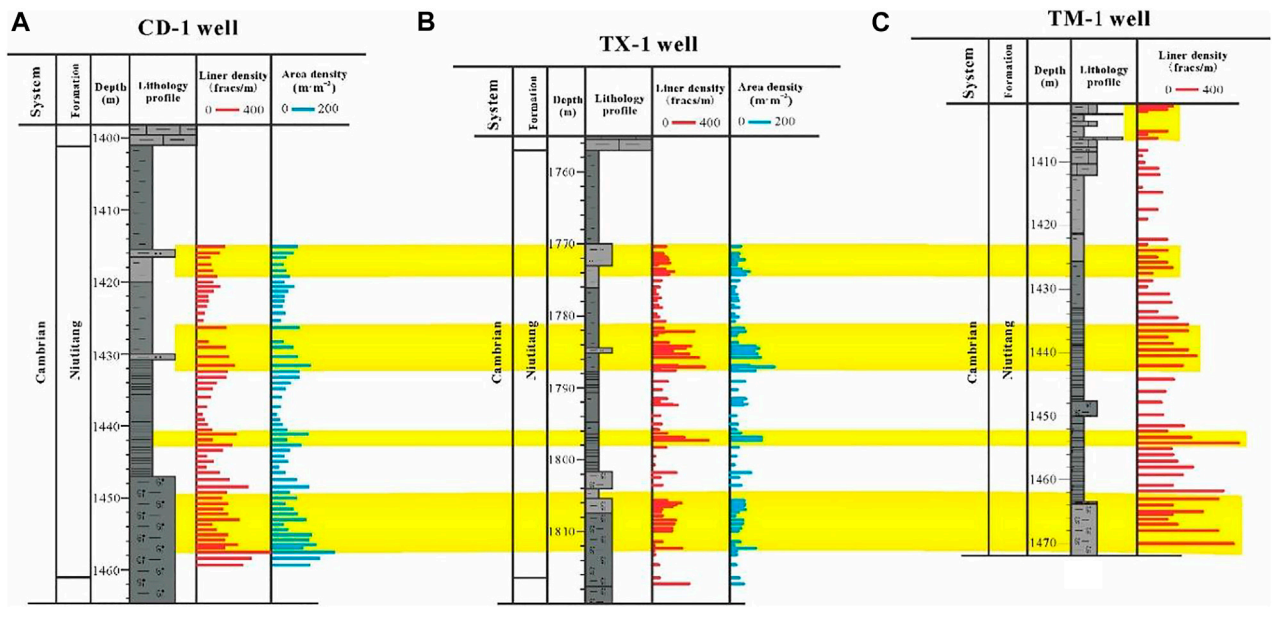

FIGURE 10 | CD-1, TX-1 and TM-1 well profiles of fracture density in Niutitang shale.

other core parameters to find out the main controlling factors of fracture development. In addition, due to the different observation personnel, observation angle, observation time, and observation degree, the fracture density of different drilling wells in different areas vary greatly, and even the fracture abundance of the same drilling well observed by different personnel is also different. Therefore, when analyzing the fracture density development characteristics, it is necessary to refer to the geological data of the study area for comprehensive analysis.

From the observation and statistics of fractures in the cores of TX-1, TM-1, and CY-1 wells in the study area (**Figure 10**), it can be seen that the fractures in the cores of the three wells approximately have the same distribution, and fracture densities are all greater in four yellow core sections. For CY-1 well, the fracture densities are calculated in the core section from 1415 to 1460 m, which shows the fractures mainly concentrated in the four core sections from 1415 to 1422 m, 1427 to 1432 m, and 1441 to 1444 m. In the core section of TX-1 well from 1770 to 1817 m, the fracture line density and area density are more obvious than those in CY-1 well, and the fractures are mainly concentrated in four core sections from 1770 to 1774 m, 1781 to 1788 m, 1796 to 1798 m, and 1806 to 1812 m, with a maximum line density of about 350 fractures/m. In addition, the core fractures in the central part of Niutitang shale are more abundant than those in the upper and lower parts. TM-1 well has the most developed core fractures among TX-1 well and CY-1 well. The fracture line density is generally larger in the whole core section (1400–1472 m), especially the core fractures at the bottom of Nititang shale are obviously more abundant than those at the middle and upper parts.

4.4 Microfractures

For shale reservoirs with ultra-low matrix porosity and permeability, the development of microfractures increases the storage space and specific surface area of free and adsorbed gas, and secondly, connects to a series of shale pore spaces such as organic pores and inorganic mineral pores, which increases the

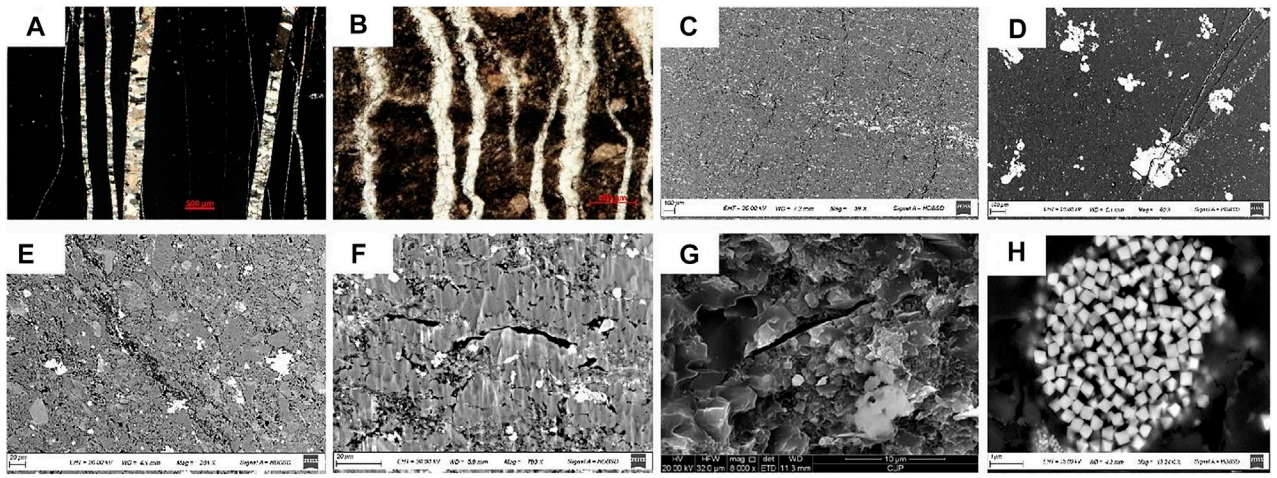

FIGURE 11 | Microfractures of Niutitang shale in Cen'gong block. **(A)** Multiparallel tectonic microfractures; **(B)** calcite-filled microfractures cutting off black argillaceous layers; **(C)** clay-filled microfractures; **(D)** tectonic microfractures cutting off pyrite; **(E)** interlayer microfractures parallel to sedimentary laminations; **(F)** grain-margin microfractures along rock particles; **(G)** intergranular microfractures of clay minerals; **(H)** intergranular pores of pyrite.

effective percolation path inside the shale and plays an important role in improving the pore permeability of the reservoir. The microfractures developed in the shales of the study area can be classified into four types, namely, tectonic microfractures, interlayer microfractures, grain-margin microfractures and intergranular microfractures, depending on the tectonic, sedimentary, and diagenetic causes as well as the developmental position (**Figure 11**).

Tectonic microfractures mainly refer to microfractures formed by extrusion, tension and other forces, whose surfaces are generally straight and often developed in groups. They are parallel to each other or cutting through each other, forming an intricate network of fractures. Tectonic microfractures can cut multiple laminations and larger rock mineral grains with greater variation in occurrence. Interlayer microfractures are also known as bedding-parallel microfractures developed along the sedimentary laminations. The extension length and aperture are both bigger than other microfractures. Grain-margin microfractures formed along the margin of mineral particles or organic matter. On the one hand, they are mainly formed by the shrinkage of organic matter and clay mineral particles, and on the other hand, due to the plasticity difference between organic matter or mineral particles with other surrounding materials, grain-margin microfractures are formed when different stresses applied. Intergranular microfractures exist between mineral wafers or grains, which can be subdivided into clay mineral intergranular microfractures and pyrite intergranular microfractures according to different mineral types. Their development is influenced by the transformation of clay minerals and recrystallization (Hu et al., 2015).

5 DISCUSSION

5.1 Bedding-Parallel Fibrous Veins

Bedding-parallel fibrous veins are widely developed in sedimentary basins, especially in shales (**Figures 8F,G**). Their formation process is closely related to the diagenesis of shales, the generation, migration, and accumulation of hydrocarbons, the property and percolation patterns of geological fluids, and the opening and closing of tectonic movements, which have attracted the attention and research of many scholars in recent years.

Although there is no clear conclusion on the formation mechanism of bedding-parallel calcite veins, most of the scholars believe that abnormal high fluid pressure is the key, and the cause of abnormally high pressure in shale is mainly the effect of organic matter hydrocarbon generation. Wang M. et al. (2020) studied the bedding-parallel fibrous veins of shales in the Dongying Depression, Bohai Bay Basin, eastern China, by examining the fibrous calcite vein and its hydrocarbon inclusion content. They verified that the bedding-parallel fibrous veins in the shale is a product of fluid overpressure caused by organic matter-generated hydrocarbon expulsion. The organic matter content of Niutitang shale in study area is very high and a large number of bedding-parallel calcite veins are generated, which indicates that Niutitang shale had a large amount of hydrocarbon production and high pressure in the early stage. This is of reference significance to the early hydrocarbon production and migration and fluid activity in the study area, and we will implement more work on this content in the future.

5.2 Fracture Characteristics and Regional Tectonic Movements

Since the formation of tectonic fractures is closely related to the remote ground stress, their fracture strike is closely related to the direction of the maximum horizontal principal stress of ground stress (Lorenz et al., 1991). The orientations of the paleostress field experienced in the study area can be roughly judged by

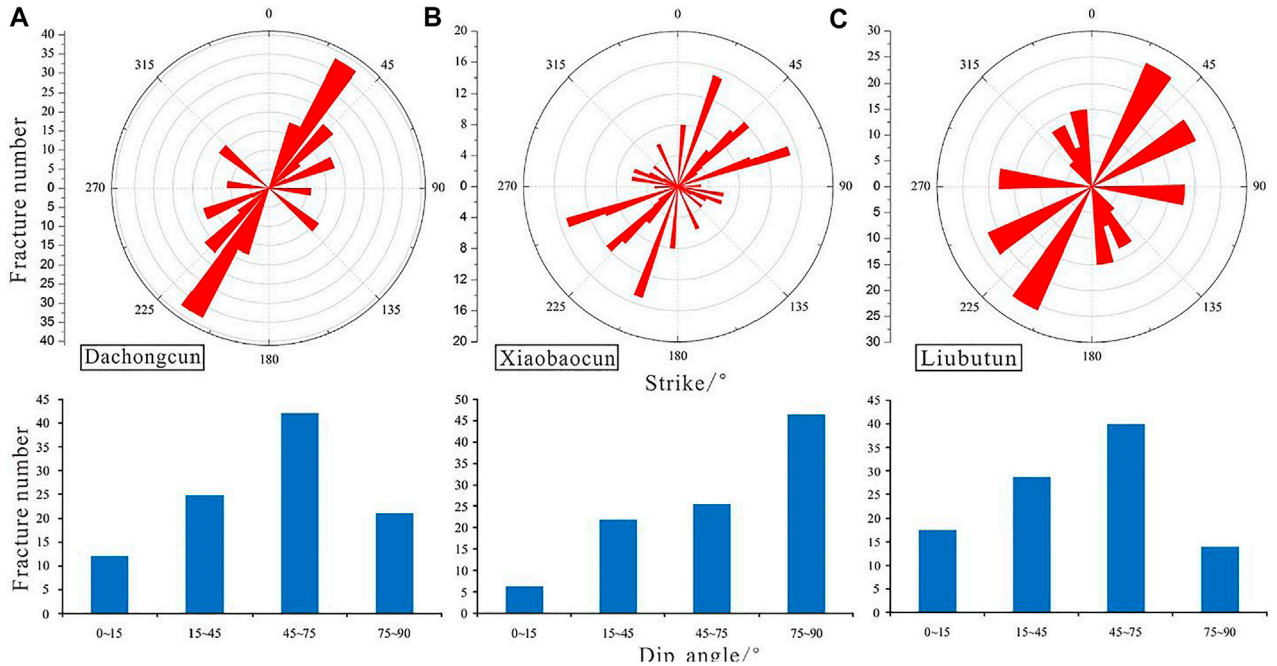

FIGURE 12 | Strikes and dips of structural fractures of Niutitang formation in three outcrops (Li et al., 2020).

counting the tectonic fracture occurrence in the Cen'gong block and drawing a rose diagram of the fracture orientation. By statistical analysis of the tectonic fracture occurrence in the Dachongcun, Xiaobaocun, and Liubutun field geological sections of the study area and the drawing of the rose diagram, the result shows that the tectonic fractures strikes are mainly in the northeast and north-northeast direction, followed by the northwest direction (**Figure 12**). It is basically consistent with the orientation of faults interpreted by the 2D seismic data of the block, indicating that the tectonic stress experienced in the study area are mainly along the northwest direction, followed by northeast direction.

The paleomagnetic orientation experiment was conducted on 21 samples from CD-1, TX-1 and TM-1 wells. Most of the samples have obvious demagnetization characteristics, and the alternating demagnetization intensity of all samples is less than 20 mT. The difference between the viscous remanence components is clearly distinguished from the primary remanence component, and some samples show only the viscous remanence component perhaps due to remagnetization, which has less impact on the experimental purpose (**Figure 13**). The experimental results show that the magnetic deflection of viscous remanence ranges from 7.4° to 342.8° and the magnetic inclination ranges from 7.1° to 66.6°, and the experimental error α95 parameters are all less than 16, showing that the experimental results have good credibility (**Figure 14**). Since the object of study is the fracture strike, the magnetic declination is fully corrected to due north, and it can be seen that the fracture strike is mainly aligned in the north-northeast direction and partly in the northwest direction, which is consistent with the directions revealed in the rose diagram of outcrop fractures.

In general, the fracture strike of the Cambrian Niutitang formation in the study area is mainly in NE and NNE, which is consistent with the early and middle Yanshanian tectonic movement. A part of fractures strike is in NW, which is consistent with Himalayan tectonic movement.

Additionally, the fracture abundance and shale gas content have a close relationship with buried depth and regional faults in study area. The Niutitang formation around TX-1 well is mostly buried at a depth of 1600–2000 m with flat strata, and less faults are developed. Drilling shows that the shales have good gas content. While the CY-1 well is closer to the fault to its north, the shales of the Niutitang formation are buried at a depth of less than 1500 m. Drilling shows that the shale gas content is general. The TM-1 well is located about 500 m from the strike-slip fault to its east, and the shales of the Niutitang formation are also buried at a depth of less than 1500 m. Drilling shows that the shale gas content is poor. A side-by-side comparison of these three wells indicates that the buried depth of shale and distance to the fault have a greater influence on the shale gas content. Furthermore, lateral comparison of the abundance of core fractures based on the fracture density data (**Figure 10**) shows that fractures in TM-1 well are most developed, followed by CY-1 and TX-1 well. Meanwhile, according to the faults map of the study area, the distance between TM-1 well and the nearest fault is less than that of CY-1 well, and CY-1 is also less than that of TX-1 well which shows that the influence of the faults on fracture abundance is evident, and the closer to the fault, the better developed the fracture is.

5.3 The Intersection Relationships and Relative Forming Time of Fractures

Although the natural fractures of the Niutitang shale in study area is numerous and various, detailed observation shows obvious

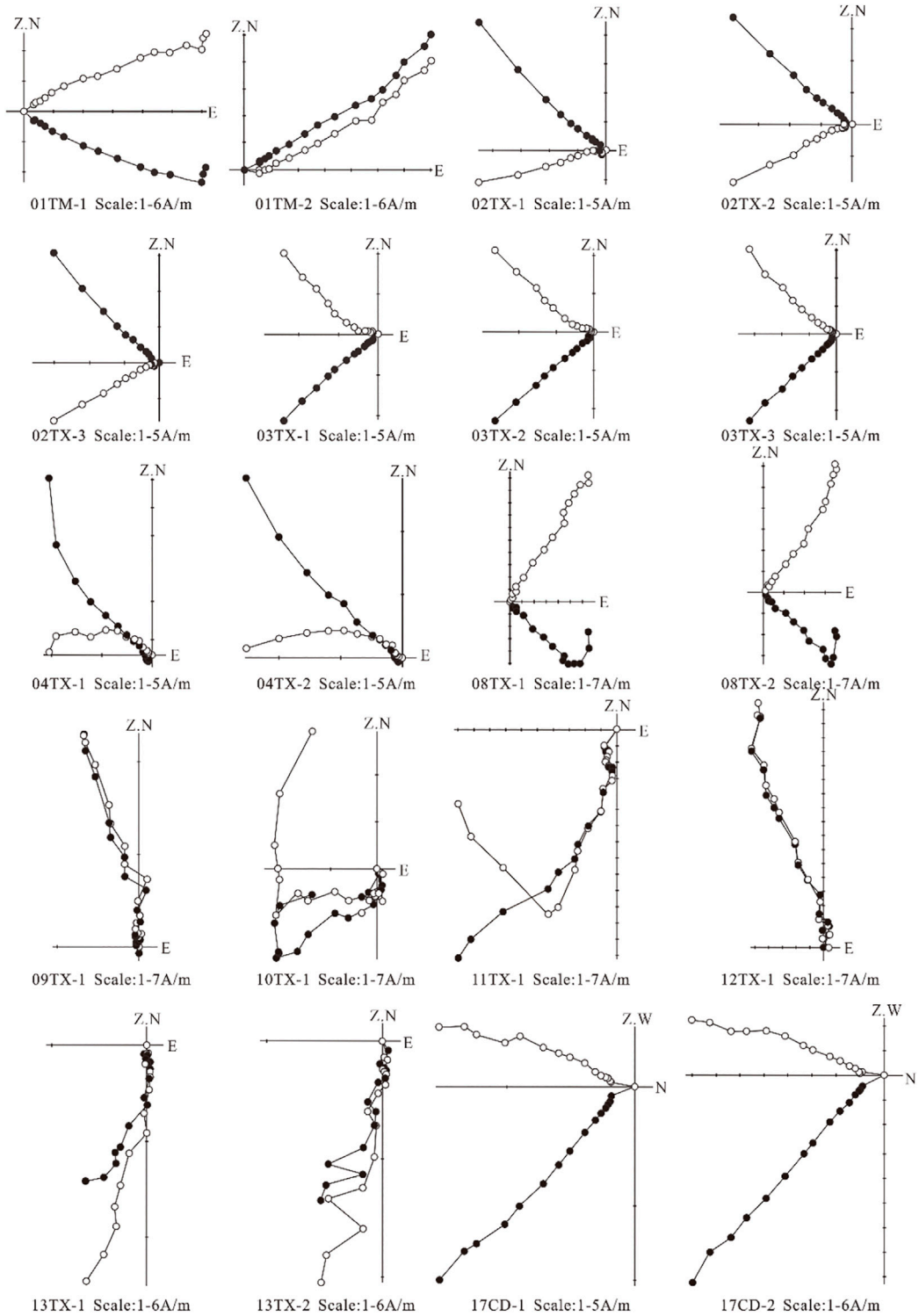

FIGURE 13 | Demagnetization curves of Niutitang shale samples in Cen'gong block.

cross-cutting relationships (**Figure 15**). The subvertical fractures cut through the horizontal pyrite-filled fractures and fibrous veins in the longitudinal direction, and consequent displacements can determine the relative motion directions. In **Figure 15A**, the pyrite nodule suffered obvious tensile deformation when cut through by vertical calcite-filled fracture, and one tip of the pyrite nodule is upwarped. According to this local deformation, it can be seen that later tectonic stress made the

Sample	Magnetic deflection/°	Magnetic inclination/°	α95
01TM-1	17.1	45.7	8.9
01TM-2	43.1	30.5	5.7
02TX-1	42	9.1	1.7
02TX-2	46.3	19.7	2.4
02TX-3	41.4	20.3	1.4
03TX-1	225.7	39	2.1
03TX-2	228.3	35.8	2
03TX-3	225.6	38	3.2
04TX-1	18.2	7.7	8.5
04TX-2	35.4	7.1	3.4
08TX-1	13.7	16.4	11.6
08TX-2	7.4	26.4	7.6
09TX-1	342.8	38.4	2.6
10TX-1	24.9	66.6	9
11TX-1	233.5	42.9	5.2
11TX-2	65.1	43.2	0
12TX-1	10.2	36.1	8.3
13TX-1	215	58.1	6.6
13TX-2	217.1	54.4	15.1
17CD-1	140.2	10.9	7.3
17CD-2	131.4	8.7	6.1

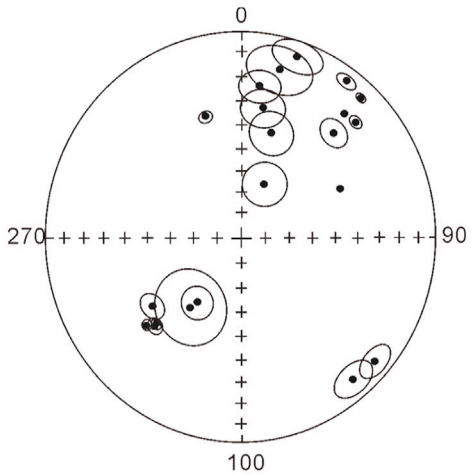

FIGURE 14 | Result of paleomagnetic orientation experiment and stereographic projection of fracture strike.

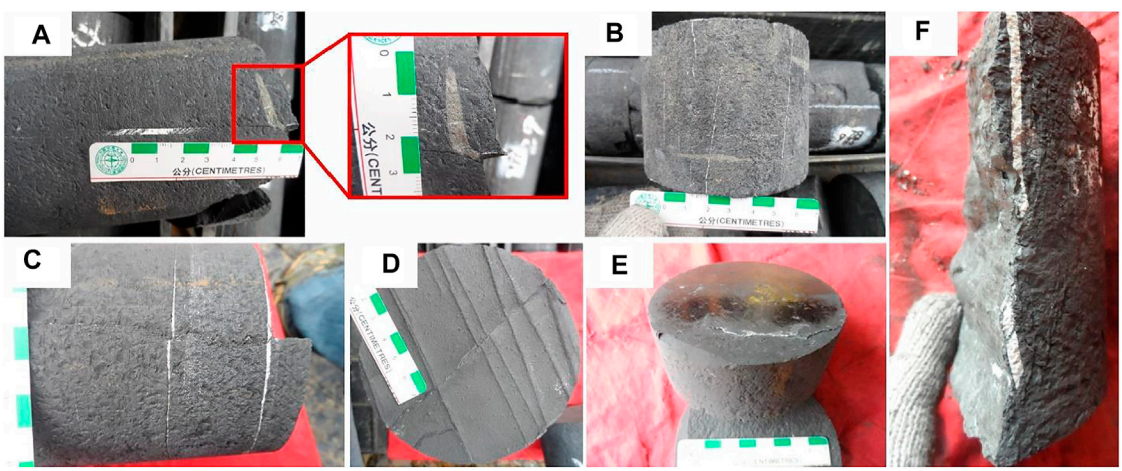

FIGURE 15 | Geometries of intersection relationship between shale fractures in Cen'gong block. **(A)** One tip of horizontal pyrite-filled fracture is upwarped by subvertical calcite-filled fracture; **(B)** subvertical fracture cutting across the horizonal pyrite-filled fracture; **(C)** one subvertical fracture cutting across two bedding-parallel fibrous veins; **(D)** intersection relationships between two subvertical fracture groups, and the included angle is about 60°; **(E)** mirror structure of slip fracture is on the top of calcite fillings of bedding-parallel fibrous vein; **(F)** subvertical slip fracture developed along the previous calcite-filled fracture.

lower shale moving along upwarped direction. When some small subvertical fractures encountered the horizontal fibrous veins or pyrite-filled fractures with bigger aperture, they tend to terminate at the contact position and no longer continue to extend; even if some of them continue to extend across horizontal fibrous veins or pyrite-filled fractures, they do not form obvious effective displacement. In addition, at least two stages of subvertical fractures formed, and later subvertical fractures cut through the early subvertical fractures in the angle ranging from approximately 60°–70°.

The early formed bedding-parallel fibrous veins and subvertical filled fractures are usually regarded as tectonic weaknesses; they are conducive to the formation of slip fractures under later shear action (**Figures 15E,F**). In the study area, there are a large number of slip

fractures formed along bedding-parallel fibrous veins or vertical calcite-filled fractures, and they have a good matching relationship with each other, and the occurrence is basically or partially the same; second, obvious calcite from bedding-parallel fibrous veins can be found under the smooth mirrors of slip fractures, and some carbonaceous mirrors are laid along the vertical calcite-filled fractures, and these structures are all well preserved as shown in **Figure 15E,F**. In addition, vertical slip fractures can be seen cutting the bedding-parallel fibrous veins. Combined with the detailed observation of the fracture types, it is clear that the horizontal pyrite-filled fractures were formed at the earliest time, followed by the bedding-parallel fibrous veins, then followed by the subvertical fractures, which were formed at least two stages and finally followed by the slip fractures.

6 SUMMARY AND CONCLUSIONS

1) The Cen'gong block is a saddle-shaped structure formed by the northeast-oriented Banxi anticline and the southwest-oriented Lannigan anticline. The Changchong syncline to the east and the Guanzhai syncline to the west further highlight the saddle-shaped features. Faults are accompanied with anticline and syncline, and most of them are along the NE and NNE direction, while few are in the EW direction.
2) Fractures in outcrops are mainly fold-fault-related fractures, bedding factures, slip fractures, and regional fractures; core fractures are mainly horizontal pyrite-filled fractures, bedding-parallel fibrous veins, subvertical fractures, and slip fractures; four types of microfractures are also defined and characterized such as tectonic microfractures, interlayer microfractures, grain-margin microfractures, and intergranular microfractures.
3) The aperture of core fractures is mainly 0.2–0.5 mm, and the length is mainly less than 10 cm. The rose diagram of three field geological sections showed that the tectonic fractures strikes are mainly in NE and NNE direction, followed by the NW direction, which is mainly consistent with the result of the paleomagnetic orientation experiment of core samples and seismic interpretation.
4) The fracture density data show that fractures in TM-1 well are the most developed, followed by CY-1 and TX-1 wells, and the distance between TM-1 well and the nearest fracture is less than that of CY-1 well, and CY-1 is also less than that of TX-1 well, which shows that the influence of the faults on fracture abundance is obvious, and the closer to the fault, the more developed the fracture is.
5) The detailed characteristics of shale fractures and intersection relationships show that the forming time of pyrite-filled fractures is earliest, followed by fibrous veins and subvertical fractures, and slip fractures are formed at the latest.

DATA AVAILABILITY STATEMENT

The original contributions presented in the study are included in the article/Supplementary Material, further inquiries can be directed to the corresponding author.

AUTHOR CONTRIBUTIONS

XW: conceptualization, methodology, formal analysis, writing–original draft, and writing–review and editing; RW: resources, methodology, investigation, supervision, and editing and revision; RG: conceptualization, methodology, supervision, and funding acquisition; AD: editing and revision; YS: methodology and funding acquisition; WD: conceptualization and methodology; YG: resources and writing–original draft; ZC: writing–review and editing. All authors reviewed the manuscript.

FUNDING

This research was supported by the National Natural Science Foundation of China (Nos. 41802151, 42172165, and 42072173), National Postdoctoral Program for Innovative Talents (No. BX201700287), and SINOPEC Ministry of Science and Technology Project (Nos. P20046-1 and P20057-1).

ACKNOWLEDGMENTS

XW acknowledges the China Scholarship Council (CSC No. 201806400035) for a joint Ph.D. fellowship, and the Energy Institute of the Pennsylvania State University for hosting and supporting his visit. We would like to thank the staff at the laboratories that helped in performing the tests and analyses. We are also grateful to the editors and reviewers for their revisions and comments.

REFERENCES

Bons, P. D., and Montenari, M. (2005). The Formation of Antitaxial Calcite Veins with Well-Developed Fibres, Oppaminda Creek, South Australia. *J. Struct. Geology.* 27 (2), 231–248. doi:10.1016/j.jsg.2004.08.009

Cai, Y., and Dahi Taleghani, A. (2019). Semi-Analytical Model for Two-phase Flowback in Complex Fracture Networks in Shale Oil Reservoirs. *Energies* 12 (24), 4746. doi:10.3390/en12244746

Cao, Z., Jiang, H., Zeng, J., Saibi, H., Lu, T., Xie, X., et al. (2021). Nanoscale Liquid Hydrocarbon Adsorption on clay Minerals: A Molecular Dynamics Simulation of Shale Oils. *Chem. Eng. J.* 420, 127578. doi:10.1016/j.cej.2020.127578

Chen, J., Wang, L., Wang, C., Yao, B., Tian, Y., and Wu, Y.-S. (2021). Automatic Fracture Optimization for Shale Gas Reservoirs Based on Gradient Descent Method and Reservoir Simulation. *Adv. Geo-energy Res.* 5 (2), 191–201. doi:10.46690/ager.2021.02.08

Dahi-Taleghani, A., and Olson, J. E. (2011). Numerical Modeling of Multistranded-Hydraulic-Fracture Propagation: Accounting for the Interaction between Induced and Natural Fractures[J]. *Spe J.* 16 (3), 575–581. doi:10.2118/124884-pa

Ding, W., Yin, S., and Wang, X. (2015). Assessment Method and Characterization of Tight sandstone Gas Reservoir Fractures[J]. *Earth Sci. Front.* 22 (4), 173–187. doi:10.13745/j.esf.2015.04.019

Dong, D., Gao, S., and Huang, J. (2014). A Discussion on the Shale Gas Exploration & Development prospect in the Sichuan Basin[J]. *Nat. Gas Industry* 34 (12), 1–15. doi:10.3787/j.issn.1000-0976.2014.12.001

Dong, D., Shi, Z., Guan, Q., Jiang, S., Zhang, M., Zhang, C., et al. (2018). Progress, Challenges and Prospects of Shale Gas Exploration in the Wufeng-Longmaxi Reservoirs in the Sichuan Basin. *Nat. Gas Industry B* 5 (5), 415–424. doi:10.1016/j.ngib.2018.04.011

English, J. M. (2012). Thermomechanical Origin of Regional Fracture Systems. *Bulletin* 96 (9), 1597–1625. doi:10.1306/01021211018

Gregory, D., Mukherjee, I., Olson, S. L., Large, R. R., Danyushevsky, L. V., Stepanov, A. S., et al. (2019). The Formation Mechanisms of Sedimentary Pyrite Nodules Determined by Trace Element and Sulfur Isotope Microanalysis. *Geochimica et Cosmochimica Acta* 259, 53–68. doi:10.1016/j.gca.2019.05.035

Guo, Y. T., Yang, C. H., Jia, C. G., Xu, J. B., Wang, L., and Li, D. (2014). Research on Hydraulic Fracturing Physical Simulation of Shale and Fracture Characterization Methods. *Chin. J. rock Mech. Eng.* 33 (1), 52–59. doi:10.13722/j.cnki.jrme.2014.01.006

Hu, Z., Du, W., and Peng, Y. (2015). Microscopic Pore Characteristics and the Source-Reservoir Relationship of Shale: A Case Study from the Wufeng and Longmaxi Formations in Southeast Sichuan Basin[J]. *Oil Gas Geology.* 36 (6), 1001–1008. doi:10.11743/ogg20150615

Jia, A., Yunsheng, W., and Jin, Y. (2016). Progress in Key Technologies for Evaluating marine Shale Gas Development in China. *Pet. Exploration Develop.* 43 (6), 949–955. doi:10.1016/s1876-3804(16)30120-3

Jin, Z., and Cai, L. (2006). Exploration Propects,problems and Strategies of marine Oil and Gas in China[J]. *Oil Gas Geology.* 27 (6), 722–730. doi:10.11743/ogg20060602

Kang, Y. (2012). Characteristics and Exploration prospect of Unconventional Shale Gas Reservoirs in China[J]. *Nat. Gas Industry* 32 (04), 1–5. doi:10.3787/j.issn.1000-0976.2012.04.001

Lan, S., Song, D., Li, Z., and Liu, Y. (2021). Experimental Study on Acoustic Emission Characteristics of Fault Slip Process Based on Damage Factor. *J. Mining Strata Control. Eng.* 3 (3), 033024. doi:10.13532/j.jmsce.cn10-1638/td.20210510.002

Li, A., Ding, W., Luo, K., Xiao, Z., Wang, R., Yin, S., et al. (2020). Application of R/S Analysis in Fracture Identification of Shale Reservoir of the Lower Cambrian Niutitang Formation in Northern Guizhou Province, South China. *Geol. J.* 55 (5), 4008–4020. doi:10.1002/gj.3648

Liu, J., Lu, M., and Sheng, G. (2021). Description of Fracture Network of Hydraulic Fracturing Vertical wells in Unconventional Reservoirs[J]. *Front. Earth Sci.* 9, 753. doi:10.3389/feart.2021.749181

Lorenz, J. C., Teufel, L. W., and Warpinski, N. R. (1991). Regional Fractures I: A Mechanism for the Formation of Regional Fractures at Depth in Flat-Lying Reservoirs [J]. *AAPG Bull.* 75 (11), 1714–1737. doi:10.1306/0c9b29e3-1710-11d7-8645000102c1865d

Seilacher, A. (2001). Concretion Morphologies Reflecting Diagenetic and Epigenetic Pathways[J]. *Sediment. Geology.* 143 (1-2), 41–57. doi:10.1016/s0037-0738(01)00092-6

Sheng, Q., and Li, W. (2016). Evaluation Method of Shale Fracability and its Application in Jiaoshiba Area. *Prog. Geophys.* 31 (4), 1473–1479. doi:10.6038/pg20160409

Taleghani, A. D., and Olson, J. E. (2014). How Natural Fractures Could Affect Hydraulic-Fracture Geometry. *SPE J.* 19 (01), 161–171. doi:10.2118/167608-pa

Wang, M., Chen, Y., Bain, W. M., Song, G., Liu, K., Zhou, Z., et al. (2020). Direct Evidence for Fluid Overpressure during Hydrocarbon Generation and Expulsion from Organic-Rich Shales[J]. *Geology* 48 (4), 374–378. doi:10.1130/g46650.1

Wang, R., Hu, Z., Long, S., Liu, G., Zhao, J., Dong, L., et al. (2019). Differential Characteristics of the Upper Ordovician-Lower Silurian Wufeng-Longmaxi Shale Reservoir and its Implications for Exploration and Development of Shale Gas In/around the Sichuan Basin. *Acta Geologica Sinica - English Edition* 93 (3), 520–535. doi:10.1111/1755-6724.13875

Wang, R. Y., Ding, W. L., Gong, D. J., Zeng, W. T., Wang, X. H., Zhou, X. H., et al. (2016). Development Characteristics and Major Controlling Factors of Shale Fractures in the Lower Cambrian Niutitang Formation, southeastern Chongqing-Northern Guizhou Area. *Acta Petrolei Sinica* 37 (7), 832–845. doi:10.7623/syxb201607002

Wang, R. Y., Hu, Z. Q., Liu, J. S., Wang, X. H., Gong, D. J., and Yang, T. (2018). Comparative Analysis of Characteristics and Controlling Factors of Fractures in marine and continental Shales: A Case Study of the Lower Cambrian in Cengong Area, Northern Guizhou Province. *Oil Gas Geology.* 39 (04), 631–640. doi:10.11743/ogg20180401

Wang, R. Y., Hu, Z. Q., and Long, S. (2022). Reservoir Characteristics and Evolution Mechanisms of the Upper Ordovician Wufeng-Lower Silurian Longmaxi Shale, Sichuan Basin[J]. *Oil Gas Geology.* 43 (2), 353–364. doi:10.11743/ogg20220209

Wang, R. Y., Hu, Z. Q., Zhou, T., Bao, H. Y., Wu, J., Du, W., et al. (2021). Characteristics of Fractures and Their Significance for Reservoirs in Wufeng-Longmaxi Shale, Sichuan Basin and its Periphery. *Oil Gas Geology.* 42 (06), 1295–1306. doi:10.11743/ogg20210605

Wang, R. Y., Nie, H. K., Hu, Z. Q., Liu, G. X., Xi, B. B., and Liu, W. X. (2020a). Controlling Effect of Pressure Evolution on Shale Gas Reservoirs: A Case Study of the Wufeng–Longmaxi Formation in the Sichuan Basin. *Nat. Gas Industry* 40 (10), 1–11. doi:10.3787/j.issn.1000-0976.2020.10.001

Wang, X., Dahi Taleghani, A., and Ding, W. (2019). Pore Structure Characteristics and its Effect on Adsorption Capacity of Niutitang marine Shale in Sangzhi Block, Southern China. *Interpretation* 7 (4), T843–T856. doi:10.1190/int-2019-0044.1

Wang, X., Ding, W., Cui, L., Wang, R., He, J., Li, A., et al. (2018). The Developmental Characteristics of Natural Fractures and Their Significance for Reservoirs in the Cambrian Niutitang marine Shale of the Sangzhi Block, Southern China. *J. Pet. Sci. Eng.* 165, 831–841. doi:10.1016/j.petrol.2018.02.042

Wang, X., Wang, R., Ding, W., Yin, S., Sun, Y., Zhou, X., et al. (2017). Development Characteristics and Dominant Factors of Fractures and Their Significance for Shale Reservoirs: A Case Study from Є1b2 in the Cen'gong Block, Southern China. *J. Pet. Sci. Eng.* 159, 988–999. doi:10.1016/j.petrol.2017.08.007

Wu, Z., Tang, M., Zuo, Y., Lou, Y., Wang, W., Liu, H., et al. (2021). Acoustic Emission-Based Numerical Simulation of Tectonic Stress Field for Tectoclase Prediction in Shale Reservoirs of the Northern Guizhou Area, China. *Energ. Geosci.* doi:10.1016/j.engeos.2021.10.005

Wu, Z., Zuo, Y., Wang, S., Chen, J., Wang, A., Liu, L., Xu, Y., Sunwen, J., Cao, J., Yu, M., Lu, C., and Wu, Y. (2017). Numerical Study of Multi-Period Palaeotectonic Stress fields in Lower Cambrian Shale Reservoirs and the Prediction of Fractures Distribution: a Case Study of the Niutitang Formation in Feng'gang No. 3 Block, South China. *Mar. Pet. Geology.* 80, 369–381. doi:10.1016/j.marpetgeo.2016.12.008

Zeng, L., and Xiao, S. (1999). Fractures in the Mudstone of Tight Reservoirs[J]. *Pet. Geology. Exp.* 21 (3), 266–269. doi:10.11781/sysydz199903266

Zhang, B., Shen, B., and Zhang, J. (2020). Experimental Study of Edge-Opened Cracks Propagation in Rock-like Materials. *J. Mining Strata Control. Eng.* 2 (3), 033035. doi:10.13532/j.jmsce.cn10-1638/td.20200313.001

Zhang, J., and Yuan, Z. (2002). Formation and Potential of Fractured Mudstone Reservoirs[J]. *Oil Gas Geology.* 23 (4), 336–338. doi:10.11743/ogg20020406

Zhou, X., Wang, R., Du, Z., Wu, J., Wu, Z., Ding, W., et al. (2022). Characteristics and Main Controlling Factors of Fractures within Highly-Evolved Marine Shale Reservoir in Strong Deformation Zone. *Front. Earth Sci.* 10, 832104. doi:10.3389/feart.2022.832104

Conflict of Interest: Authors XW, RW, RG, YS, YG, and ZC were employed by China Petroleum & Chemical Corporation (SINOPEC). Author SS was employed by Beijing Jiaoen Energy Exploration Co., Ltd.

The remaining authors declare that the research was conducted without any commercial or financial relationships that could be construed as a potential conflict of interest.